Chain Length Effect on the Structure and Photoelectrochemical Properties of Self-Assembled Monolayers of Porphyrins on Gold Electrodes

Hiroshi Imahori,*,§ Hiroyuki Norieda, Yoshinobu Nishimura,‡ Iwao Yamazaki,*,‡ Kazuo Higuchi,*,† Naohiko Kato,† Tomoyoshi Motohiro,† Hiroko Yamada, Koichi Tamaki, Masatoshi Arimura, and Yoshiteru Sakata*

The Institute of Scientific and Industrial Research, Osaka University, 8-1 Mihoga-oka, Ibaraki, Osaka 567-0047, Japan

Received: August 4, 1999; In Final Form: October 26, 1999

Disulfides, with a systematic series of alkyl spacers containing porphyrins at both terminals, were prepared to investigate the effect of the spacer length on the structure and photoelectrochemical properties of self-assembled monolayers (SAMs) of the porphyrins on a gold electrode. The structure of the SAMs was studied using ultraviolet (UV)−visible absorption spectroscopy in transmission mode, cyclic voltammetry, UV−visible ellipsometry, and fluorescence spectroscopy. These measurements showed that as the length of the spacers increases, the SAMs tend to form highly ordered structures on the gold electrodes. In addition, the structures of the monolayers vary depending on the even and odd number of the methylene spacers (*n*). From these measurements a porphyrin dimer model is proposed in that the two porphyrins take J-aggregate-like partially stacked structures in the monolayers. Photoelectrochemical studies were carried out in argon-saturated Na_2SO_4 aqueous solution containing methyl viologen as an electron carrier using the modified gold working electrode, a platinum wire counter electrode, and a Ag/AgCl reference electrode. The quantum yield increases in a zigzag fashion with an increase in the spacer length up to $n = 6$ and then starts decreasing slightly as the chain lengths become longer. A plausible explanation for the photocurrent trend comes from the following points: (i) there are two competitive deactivation pathways for the excited singlet state of the porphyrin dimer, i.e., the quenching by the electrode via energy transfer and by the electron carrier via electron transfer, (ii) the porphyrin aggregation enhances the rate of nonradiative pathway in the excited state, and (iii) the electron transfer rate from the gold electrode to the resulting porphyrin cation radical decreases with an increase of the spacer lengths. These results will provide basic information for the construction of molecular assembly with photoactive function on surface.

Introduction

Organized molecular assemblies are of much interest because of the unique properties not seen in a single molecule. Photosynthesis is among the most typical examples of sophisticated molecular assemblies in nature. Well-defined aggregates of chlorophylls and carotenoids in antenna complexes of photosynthesis are responsible for the light harvesting and subsequent vectorial energy transport to the chlorophyll dimer in the reaction center. The following multistep electron transfer (ET) takes place from the dimer to the quinones along the well-arranged pigments embedded in the protein matrix, leading to the generation of a long-lived, charge-separated state with nearly 100% quantum yield. Thus, molecular assemblies, accomplished by the surrounding proteins and lipid membranes, are one of the key factors to control the efficient energy transfer (EN) and ET in nature. The importance of molecular aggregates in nature has prompted us to assemble functional molecules in an artificial manner without the help of proteins. So far there have been numerous attempts to organize molecules using a variety of techniques such as Langmuir−Blodgett (LB) films and lipid membranes.[1] However, the instability and the defect have hampered practical application of these systems to molecular devices.

Self-assembled monolayers (SAMs) have become a subject of intense interest in materials science and molecular technologies, because they provide highly ordered structures on surfaces.[1a,2] SAMs comprising hydrocarbons bound to a gold surface via a S−Au linkage are the most widely studied systems for the understanding of the fundamental properties of the SAMs. There are a number of reports on the SAMs dealing with the chain length effect, where the relationship between the hydrocarbon chains and the structure of the SAMs is well established. Based on the results, covalent attachment of functional molecules to the terminal of SAMs has been pursued to construct well-organized molecular assemblies containing photo- and/or electroactive molecules on gold electrodes. So far a variety of examples using ferrocenes,[3] azobenzenes,[4] porphyrins,[5] fullerenes,[6] and others[7] have appeared. However, the chain length effect on the functionalized SAMs remains obscure when relatively large functional chromophores such as porphyrins and fullerenes are employed, compared to small redox-active molecules such as ferrocenes. This is because not only the interaction among the methylene chains affects the structure, but also the interaction among the chromophores contributes it greatly.

† Toyota Central R&D Laboratories, Inc., Nagakute, Aichi 480-1192, Japan.

‡ Department of Molecular Chemistry, Graduate School of Engineering, Hokkaido University, Sapporo 060-8628, Japan.

§ Present address: Department of Material and Life Science, Graduate School of Engineering, Osaka University, Suita, Osaka 565-0871, Japan.

10.1021/jp992768f CCC: $19.00
Published on Web 01/25/2000

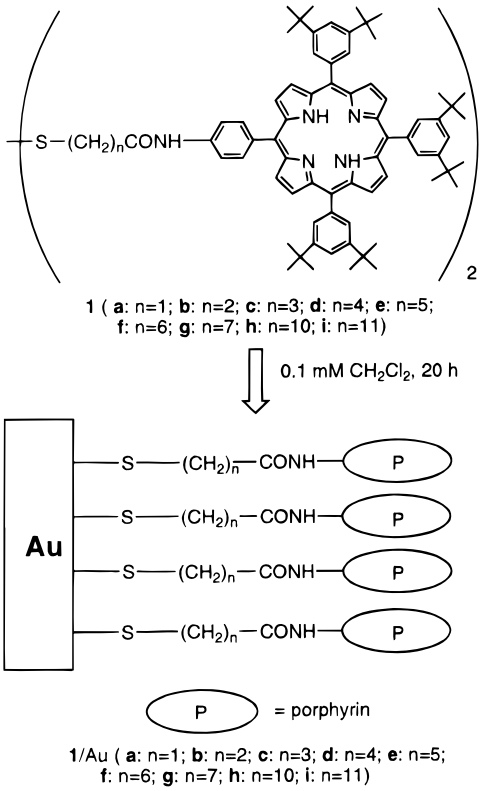

Figure 1. Self-assembled monolayers of porphyrins **1a**−**i** on gold electrodes.

Here we report on the structure and photoelectrochemistry of SAMs of porphyrins on gold electrodes (Figure 1). It is known that thiols and disulfides covalently bind to a gold surface, whereas porphyrins bearing a thiol group are susceptible to be oxidized by oxygen and/or light. To avoid such a situation, we designed disulfide **1** where two porphyrins are linked via a symmetrical dialkyl disulfide spacer. In the molecular design of **1**, six *tert*-butyl groups were introduced into *meso*-phenyl rings of the porphyrin moiety to increase the solubility in organic solvents and to regulate the interaction among the porphyrins in the monolayers. Comprehensive studies on the present systems will provide basic information for the construction of molecular photonics as well as of photosynthetic antenna system. The effect of the chain length on the SAMs was systematically investigated using the UV−visible absorption spectroscopy, cyclic voltammetry, UV−visible ellipsometry, fluorescence spectroscopy, and photoelectrochemistry. We will describe possible structural models based on the results. The chain length effect on the photophysical and photoelectrochemical properties of the porphyrins on gold electrodes will be discussed in detail.

Experimental Section

Materials and Preparation. Synthesis and characterization of **1** are described in Supporting Information. Gold electrodes were prepared by a vacuum deposition technique with chromium (50−100 Å) and gold (200−1000 Å) in a sequence onto Si (100) wafers (Sumitomo Sitix Corp.) or with gold (1000 Å) onto fresh mica (ca. 1−3 cm × 1−3 cm). Atomic force microscopy (AFM), scanning tunneling microscopy (STM), and X-ray diffraction studies showed that the gold electrodes have mainly (111) surface. The roughness factor (1.1) both for the systems was estimated by iodine chemisorption on Au(111) surface. The gold-coated wafers (Au/Cr/Si) were cut into slides (ca. 1−3 cm × 1−3 cm), rinsed with dilute hydrochloric acid, Millipore water, and ethanol and dried with a stream of argon before being soaked in a solution of disulfides. The gold electrodes on mica (Au/mica) were annealed with hydrogen flame for 30 s immediately prior to immersion into the solutions. Adsorption was carried out from dichloromethane solutions of 1.0×10^{-4} M at 25 °C for 20 h to reach the equilibrium. The time profile of the amount of the adsorbed molecules on the gold substrate was monitored using the UV−visible absorption spectroscopy to confirm the complete formation of the monolayers. After soaking, the electrode was washed well with dichloromethane and ethanol and dried with a stream of argon.

Experimental Conditions. UV−visible spectra in solutions were obtained on a Shimadzu UV3000 spectrometer, while those on gold electrodes (Au/glass: 200 Å on transparent glass slide (Matsunami), roughness factor = 1.5) were recorded on a Hitachi U-3500 spectrometer in transmission mode. The ellipsometric data have been obtained using a Rudolph Research S2000 Spectroscopic Ellipsometer. The source is a high-pressure Xe short arc lamp. The samples have been measured under the following conditions; 70 degree both incident and reflection angles, 5 mm beam size, 300 to 800 nm spectral range. The optical constants and thicknesses were fitted by using a uniform-film model and Newton's gradient method. The optical constants of the monolayers were determined by fitting with the ellipsometric parameters for the clean gold as bare substrate and for the monolayer-modified gold as samples, where a thickness of 36 Å was assumed for densely packed porphyrins monolayer ($n = 11$) which have a methylene spacer 30 degree from the substrate normal. Then the thicknesses of monolayers ($n = 1-10$) were fitted with the ellipsometric parameters of the substrate and the monolayers by applying the optical constants of the monolayer ($n = 11$).

All electrochemical studies were performed on a Bioanalytical Systems, Inc. CV-50W voltammetric analyzer using a standard three-electrode cell with a modified Au working electrode (0.48 cm^2), platinum wire counter electrode, and a Ag/AgCl (saturated KCl) reference electrode. Photoelectrochemical measurements were performed in a one-compartment Pyrex UV cell (5 mL) under argon atmosphere. The cell was illuminated with monochromatic excitation light through interference filters (MIF-S, Vacuum Optics Corporation of Japan) by 180 W UV lamp (Sumida LS-140UV) on the SAM of 0.48 cm^2. Unless otherwise stated, an argon-saturated 0.1 M Na_2SO_4 and 5×10^{-3} M methyl viologen aqueous electrolyte solution was used. The photocurrent was measured in a three-electrode arrangement, a modified gold working electrode, a platinum wire counter electrode (the distance between the electrodes is 0.3 mm), and a Ag/AgCl (saturated KCl) reference. The light intensity was monitored by an Anritsu ML9002A optical power meter.

Corrected fluorescence spectra in solutions and on gold electrodes were taken using a SPEX Fluorolog 2 spectrometer. Fluorescence decay curves on gold surfaces and in solutions were measured by means of a time-correlated single photon counting method using the second harmonic (435 nm) of Ti: sapphire laser (Coherent MIRA 900).[8]

Results

Spectroscopic Studies on Porphyrin SAMs. Figure 2 shows the absorption spectra of **1i**/Au/glass ($n = 11$) in transmission mode and of **1i** in CH_2Cl_2. The Soret band on the gold surface is broadened and red-shifted by 7 nm relative to the corresponding spectra in CH_2Cl_2. Similar behavior was observed for **1a**−**h**/Au/glass. The results are summarized in Table 1. The four porphyrin Q bands were also observed. However, owing

TABLE 1: Results Obtained Using UV−Visible Absorption Spectroscopy in Transmission Mode, Cyclic Voltammetry, and UV−Visible Ellipsometry

system	absorbance[a]	$\lambda_{max/nm}$[b]	$\Gamma/10^{-10}$ mol cm^{-2},[d] (molecular area /Å^2 molecule^{-1})	ellipsometric thickness /Å[e]	theoretical thickness /Å[f]
1a/Au ($n = 1$)	0.017	425	0.77 (220)	9.2	26
1b/Au ($n = 2$)	0.023	425	1.2 (140)	11.5	17
1c/Au ($n = 3$)	0.021	425	0.98 (170)	18.2	28
1d/Au ($n = 4$)	0.021	425	1.0 (170)	18.2	19
1e/Au ($n = 5$)	0.032	427	1.4 (120)	24.3	30
1f/Au ($n = 6$)	0.029	427	1.3 (130)	24.6	21
1g/Au ($n = 7$)	0.034	427	1.5 (110)	31.8	32
1h/Au ($n = 10$)	0.036	428	1.5 (110)	26.0	25
1i/Au ($n = 11$)	0.034	428	1.5 (110)	36.0	36
1i		421[c]			

[a] Absorbance at the Soret band. [b] λ_{max} at the Soret peak. [c] Measured in CH_2Cl_2. [d] Surface coverage obtained using cyclic voltammetry. [e] Ellipsometrically determined. [f] Estimated using CPK model, assuming that the porphyrins are densely packed with a methylene spacer 30° from the surface normal.

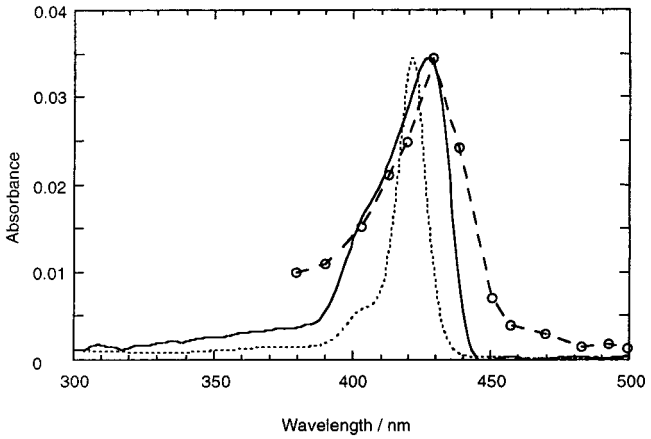

Figure 2. UV−visible absorption spectra of **1i**/Au/glass in transmission mode ($n = 11$, solid line) and of **1i** in dichloromethane (dotted line) and action spectrum in mica/Au/**1i**/MV^{2+}/Pt cell (dashed line with circles). The spectra are normalized at the Soret band for comparison.

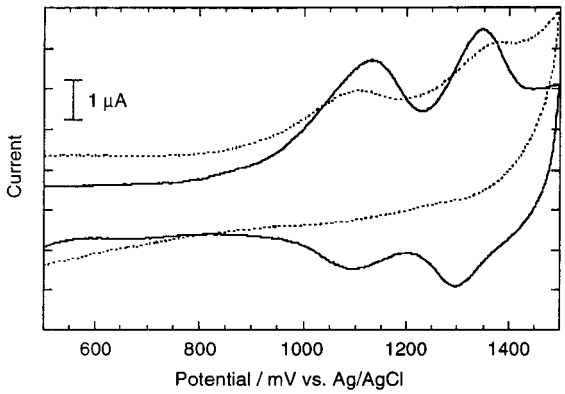

Figure 3. Cyclic voltammograms of **1a**/Au/mica ($n = 1$, dotted line) and **1i**/Au/mica ($n = 11$, solid line) in dichloromethane: 50 mV s^{-1}; electrode area, 0.48 cm^2.

to the poor signal-to-noise ratio of the Q bands on gold electrodes, it was quite difficult to obtain reliable spectra at the wavelength longer than 500 nm. Similar red-shift and broadening of the Soret band were reported for porphyrin SAMs on gold electrodes,[5] LB monolayers of porphyrins on glass or semiconductors,[9] and porphyrin aggregates in solutions.[10] It is well known that a stacked face-to-face porphyrin π-aggregation (sandwich-type H-aggregate) leads to a blue shift, while side-by-side porphyrin π-aggregation (J-aggregate) leads to a red shift.[10,11] Thus, the spectral change is probably due to the J-aggregate-like partially stacked structures of the porphyrins in the monolayer microenvironment. The red-shift of the Soret band on gold electrodes is relatively small, compared with the similar porphyrin aggregates,[9−11] indicating the moderate interaction among the porphyrins. The absorbance at the Soret band increases gradually with an increase in the number of methylenes ($n = 1-7$), while **1g**−**i**/Au/glass ($n = 7$, 10, 11) does not exhibit a substantial change in the intensities. Assuming that the molar absorption coefficients of **1a**−**i**/Au/glass are similar, this suggests that the amounts of the adsorbed molecules become saturated at around $n = 7$. There is a zigzag trend on the changes in the absorbance with an increase of the number of the methylene groups, implying that the even-and-odd number of the methylene groups is a crucial factor for the monolayer structures. A small red shift (up to 3 nm) of the Soret band peak position (λ_{max}) was observed as the chains became longer (Table 1). The changes correlate well with those in the absorbance. This shift may be ascribed to an increase in the $\pi-\pi$ interaction among the porphyrin moieties, but the existence of the bulky *tert*-butyl groups at the *meso*-phenyl groups does not allow the porphyrins interact intensively. The thicknesses of the SAMs were measured by UV−visible spectroscopic ellipsometry. The determined thicknesses for **1a**−**i**/Au/Cr/Si are 9−36 Å, indicating the formation of the monolayers, as shown in Table 1. A zigzag tendency on the changes in the thicknesses as a function of the number of the methylenes is seen, similar to that of the UV−visible spectra on gold electrodes, which will be discussed later.

Electrochemistry. Cyclic voltammetry of **1a**−**i**/Au/mica was performed in CH_2Cl_2 containing 0.1 M *n*-Bu_4NPF_6 with a sweep rate of 50 mV s^{-1}. A typical example is shown in Figure 3. Two successive redox couples, corresponding to the first and the second oxidation/re-reduction of the porphyrin moiety ($E_{1/2}$ = +1.10, +1.33 V vs Ag/AgCl), were clearly seen for **1i**/Au/mica. Similar redox behavior was observed for **1b**−**h**/Au/mica (Table 2). On the other hand, the redox waves were completely irreversible for **1a**/Au/mica, indicating the poor packing of the porphyrins on gold electrodes (Figure 3). The cyclic voltammetric curve of 5-(4-acetoamidophenyl)-10,15,20-tris(3,5-di-*tert*-butylphenyl)porphyrin **2** (Chart 1) in the CH_2Cl_2 solution displayed features characteristic of a diffusional, reversible process ($E_{1/2}$ = +0.91, +1.25 V vs Ag/AgCl). The oxidation potentials of **2** in CH_2Cl_2 are shifted more negative by 140−190 mV compared to those of **1b**−**i**/Au/mica. This difference is likely a consequence of the decreased dielectric constant in the diffuse monolayer as compared with that of bulk solution. Integration of the area under the anodic surface waves due to

TABLE 2: Results Obtained Using Cyclic Voltammetry and Fluorescence Lifetime and Photoelectrochemical Measurements

system	$E_{1/2}^{0/+1}$/V[a] (ΔE_{peak}/V)[b]	$E_{1/2}^{+1/+2}$/V[a] (ΔE_{peak}/V)[b]	$\tau_{f/ns}$[d]	photocurrent intensity /nA[f]	quantum yield /%[f]
1a/Au ($n = 1$)	*c*	*c*	0.015	93	0.095
1b/Au ($n = 2$)	1.07 (0.07)	1.31 (0.09)	0.013	75	0.057
1c/Au ($n = 3$)	1.05 (0.08)	1.32 (0.04)	0.016	320	0.27
1d/Au ($n = 4$)	1.06 (0.08)	1.31 (0.07)	0.015	290	0.23
1e/Au ($n = 5$)	1.08 (0.07)	1.33 (0.07)	0.021	660	0.33
1f/Au ($n = 6$)	1.10 (0.06)	1.31 (0.07)	0.021	620	0.34
1g/Au ($n = 7$)	1.10 (0.07)	1.33 (0.09)	0.024	600	0.33
1h/Au ($n = 10$)	1.10 (0.04)	1.32 (0.05)	0.040	680	0.30
1i/Au ($n = 11$)	1.10 (0.04)	1.33 (0.04)	0.040	660	0.30
2	0.91	1.25	9.8[e]		

[a] Measured in CH_2Cl_2 containing 0.1 M *n*-Bu_4NPF_6 with a sweep rate of 50 mV s^{-1} using a Ag/AgCl (saturated KCl) reference. [b] Peak separation between the anodic and cathodic peaks. [c] Re-reduction waves due to the porphyrin were not observed. [d] Obtained using single photon counting fluorescence lifetime technique when excited at 435 nm and monitored at 655 nm. [e] Measured in THF. [f] Obtained in the three electrode systems under excitation with $\lambda = 428.8 \pm 3.9$ nm light of 6.0 mW cm^{-2} and −200 mV vs Ag/AgCl bias voltage.

CHART 1

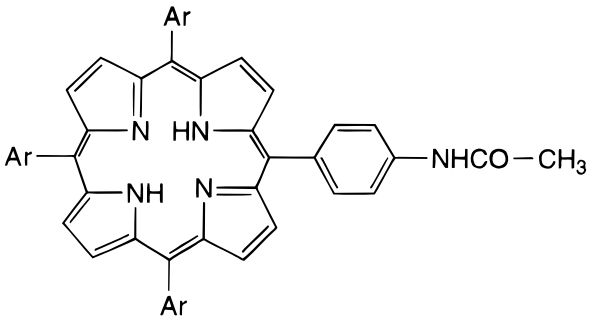

2 Ar=3,5-(*t*-Bu)$_2$C$_6$H$_3$

the first oxidation of the porphyrin provides an estimate of the surface coverage, Γ, after correcting for surface roughness (roughness factor = 1.1). The results are summarized in Table 1. There is a similar tendency between the changes in the Γ values and the absorbance as a function of the number of the methylene groups. The Γ values ($0.77-1.5 \times 10^{-10}$ mol cm^{-2}) obtained here using the cyclic voltammetry are quite consistent with those ($0.4-2.0 \times 10^{-10}$ mol cm^{-2}) of the similar porphyrin SAMs reported previously.[5,12] Provided that the porphyrins as a cubic molecule are packed densely with a perpendicular orientation to the gold surface, then the area of one molecule is calculated to be ca. 200 Å^2 (20 Å × 10 Å). The values of the molecular areas for **1g**−**i**/Au/mica (110 Å^2) is somewhat smaller than the expected value (200 Å^2). If the bulky *tert*-butyl groups are absent on the *meso*-pheyl groups at the porphyrin ring, the area of one molecule is estimated to be ca. 50 Å^2. Thus, it is concluded for **1g**−**i**/Au/mica that the porphyrins are well packed, reducing the free volume among the porphyrins. However, the values of molecular areas for **1a**−**f**/Au/mica (120−220 Å^2) are still much smaller than a value (400 Å^2) where the porphyrins are densely packed with a parallel orientation to the gold surface. Considering the porphyrin aggregation observed using the UV−visible absorption spectroscopy, the porphyrins may be tilted from the surface normal to some extent, sustaining the significant interaction among the porphyrins for **1a**−**f**/Au/mica.

Photoelectrochemical Studies and Fluorescence Spectroscopy. Photoelectrochemical measurements were carried out for **1a**−**i**/Au/mica in Ar-saturated 0.1 M Na_2SO_4 aqueous solution containing 5 mM methyl viologen (MV^{2+}) as an electron carrier using the modified gold electrode as a working electrode, a platinum counter electrode, and a Ag/AgCl reference electrode (hereafter, mica/Au/**1a**−**i**/MV^{2+}/Pt, where "/" represents an interface). Figure 4 shows currents produced by on-and-off illumination of the mica/Au/**1i**/MV^{2+}/Pt cell as a function of the applied potential under the excitation of light at a wavelength of 428.8 (± 3.9) nm with a power density of 6.0 mW cm^{-2}. The SAM showed a photoelectronic response when switching the light on and off. The intensity of the net photocurrent for the mica/Au/**1i**/MV^{2+}/Pt cell is at least an order of magnitude larger than that of mica/bare Au/MV^{2+}/Pt cell, indicating the involvement of the porphyrin for the photocurrent generation. O_2 bubbling of the solution increased the photocurrent by ca. 20−30%, and successive Ar bubbling of the solution decreased it nearly to the initial state both in the absence and the presence of MV^{2+}. The results indicate that O_2 is an efficient electron carrier in the present system.[6c] Addition of MV^{2+} (up to 5 mM) increased the photocurrent by about 15%, showing that MV^{2+} is also an electron carrier.[6c] However, further addition of MV^{2+} did not change the intensity of the photocurrent. The intensity of the photocurrent was maintained almost constant during the irradiation at least 2 h. There is a good linear relationship between the intensities of the photocurrent and of the light at each wavelength (from 0.03 to 6.0 mW cm^{-2}). In the three electrode systems, an increase in the net cathodic photocurrent with an increase of the negative bias (from 700 mV to −200 mV) to the gold electrode demonstrates that the photocurrent flows from the gold electrode to the counter electrode through the SAM and the electrolyte. The dark current is much lower than the net photocurrent within the range of the applied

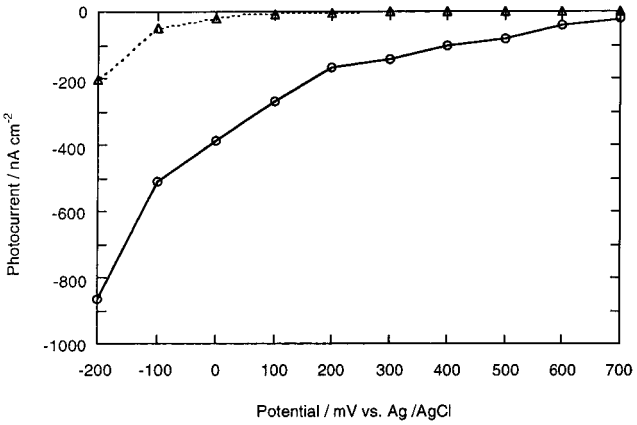

Figure 4. Photocurrent vs applied potential curves for mica/Au/**1i** ($n = 11$) /MV^{2+}/Pt cell (solid line with circle) with a monochromic light of 428.8 nm with 6.0 mW cm^{-2}: working electrode, **1i**/Au; counter electrode, Pt; reference electrode, Ag/AgCl (saturated KCl); electrolyte, 0.1 M Na_2SO_4 containing 5 mM methyl viologen under argon atmosphere. The dark current is shown as dotted line with triangle.

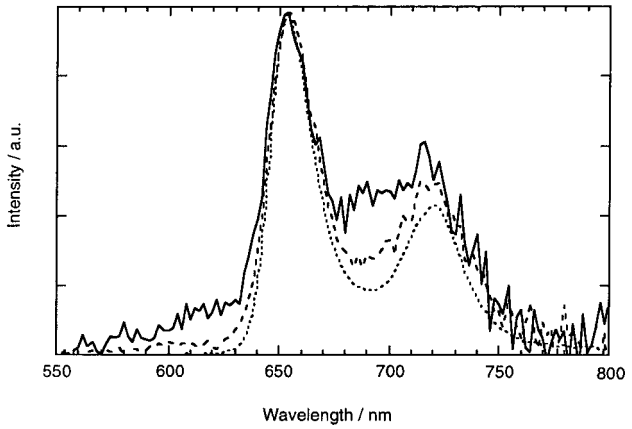

Figure 5. Corrected fluorescence spectra of **1a**/Au/Cr/Si ($n = 1$, solid line), **1i**/Au/Cr/Si ($n = 11$, dashed line), and **2** (dotted line) in CH_2Cl_2. The spectra are normalized for comparison.

potential to the gold electrode. However, when the more negative or the positive potential was applied for the system, the photoelectrochemical response was not reproducible, implying the collapse of the monolayer structure. Under the excitation of light at a wavelength of 428.8 (± 3.9) nm with a power density of 6.0 mW cm^{-2} at −200 mV bias voltage, we obtained a net current density of 660 nA cm^{-2}. Given an absorbance of 0.046 including the reflection at 428.8 nm for the **1i**/Au, we can estimate the quantum yield of the mica/Au/**1i**/MV^{2+}/Pt cell to be 0.30%. The action spectrum roughly agrees with the absorption spectrum of **1**/Au/glass in the range of 380−500 nm, showing that the porphyrin is the photoactive species (Figure 2). The small difference in shape and the peak position between the two spectra may be due to the difference between the actual spectrum obtained in transmission mode in air and the real spectrum on gold surface under the photoelectrochemical conditions, where the porphyrins are in contact with the electrolyte solution. Similar photoelectrochemical behavior was observed for the **1a**−**h**/Au/mica cells. However, dark cathodic current becomes more prominent as the number of methylene groups decreases, indicating direct electron flow from gold electrode to the electrolyte due to the loose packing of the monolayers. The intensities of the net photocurrents at −200 mV and the quantum yields are summarized in Table 2. The intensities of the photocurrent in the mica/Au/**1**/MV^{2+}/Pt cell exhibited an even-and-odd dependence on the number of the methylene groups in the chain. They became saturated at around $n = 6$, and then decreased gradually ($n = 7$, 10, 11). Such a trend is clearly seen for the quantum yields (Table 2).

Steady-state corrected fluorescence spectra of **1a**−**i**/Au and **2** in CH_2Cl_2 were taken by exciting at 427 nm. The emission spectra of **1a**/Au/Cr/Si, **1i**/Au/Cr/Si, and **2** in dichloromethane are shown in Figure 5. The peak positions as well as the shape of the emissions are quite similar. A similar tendency was observed for **1a**−**h**/Au/Cr/Si. However, the spectra become broader in the order of **2** in CH_2Cl_2 and **1i**−**a**/Au/Cr/Si, suggesting the existence of the aggregation among the porphyrins in the monolayers and/or interaction between the porphyrins and the gold surface. Time-resolved, single-photon counting fluorescence studies were made for **1a**−**i**/Au/Cr/Si and **2** in solutions with excitation at 435 nm. The decay curves at 655 nm could be fitted as single exponential, implying the existence of a single form of the aggregated porphyrins in the monolayers (Table 2). The fluorescence lifetimes of **1a**−**i**/Au/Cr/Si (13−40 ps) were much shorter than those of **2** in THF (9.8 ns) and benzene (9.7 ns), indicating that the excited singlet state of the porphyrin is quenched by the gold surface and that the nonradiative decay is enhanced by the aggregation, which will be discussed later.

Discussion

Structures of Porphyrin SAMs. UV−visible ellipsometry and electrochemical studies, as well as UV−visible absorption spectroscopy, have established the structure of the porphyrin monolayers. As the number of the methylene groups increases, the amount of the adsorbed molecules increases, showing that van der Waals interaction among the methylene spacer strongly contributes to the formation of the monolayers, similar to alkanethiol SAMs on gold surface. However, the values of the surface coverage do not increase linearly with an increase of the spacer lengths. Dependence of the even-and-odd number of the methylenes on the surface coverage was observed clearly for **1a**−**i**/Au. The spectroscopic and electrochemical origin of this even−odd progression can be explained as shown in Figure 6. Assuming that the spacer with even number of the methylenes is oriented at an angle of 30° from the surface normal, the porphyrin plane is tilted heavily to the gold surface. On the other hand, the porphyrin is almost perpendicular to the gold surface when the spacer has the odd number of the methylene. Based on the models, the structures of the monolayers with the long methylene spacers ($n = 7$, 10, 11) can be understood reasonably. In fact, there is a good agreement between the ellipsometric and the estimated thicknesses. These models are quite consistent with Fourier transform infrared spectroscopy (FTIR) in the alkanethiol SAMs on gold and silver surface where the terminal methyl orientation changes depending on the even-and-odd number of the methylene groups.[13] Although there is detectable difference due to the even-and-odd effect in the shape of the FTIR spectra in our systems, we could not assign the peaks because of the complicated and overlapped signals. The area of an alkyl chain is estimated to be ca. 20 $Å^2$, whereas that of the porphyrin is up to 110 $Å^2$. This means that if the alkyl chains were all-trans, even tilted at an angle of 30° from the surface normal, there should be a significant free volume in the alkyl spacer region of the SAM. As we described later, the preliminary dilution experiment on mixed SAMs using alkanethiols with the same chain length of the spacer and **1** displayed still significant aggregation of the porphyrins in the monolayers on the basis of the absorption spectra on the gold surface. Thus, we could not obtain any evidence for the order of the alkyl groups. Since both the porphyrin and the alkyl spacer have hydrogen atoms, it is impossible to differentiate the C−H bands in the FTIR spectra for the determination of the order of the alkyl groups. Preliminary AFM studies showed that the porphyrins are arranged with a separation of ca. 10−20 Å for **1g** ($n = 7$) /Au/mica, whereas large domain structures (ca. 200−400 × 200−400 $Å^2$) were observed for **1h** ($n = 10$) /Au/mica. From CPK modeling the shortest interplane distance between the two porphyrins is estimated to be ca. 6 Å when the two porphyrin planes are parallel and the *tert*-butyl group on the *meso*-phenyl ring is in van der Waals contact with the center of the other porphyrin plane. Single-crystal diffraction studies for similar *meso*-tetraphenylporphyrins with eight *tert*-butyl groups on the meta positions of the phenyl rings[14] showed that the mean interplane distance is ca. 7 Å where the packing structure is similar to that for the CPK modeling. These values roughly agree with the well-packed structure of the porphyrins on the gold surface. On the other hand, there is a significant deviation between the values of the theoretical and ellipsometric thicknesses for **1a**−**f**/Au ($n = 1$−6). Considering the existence

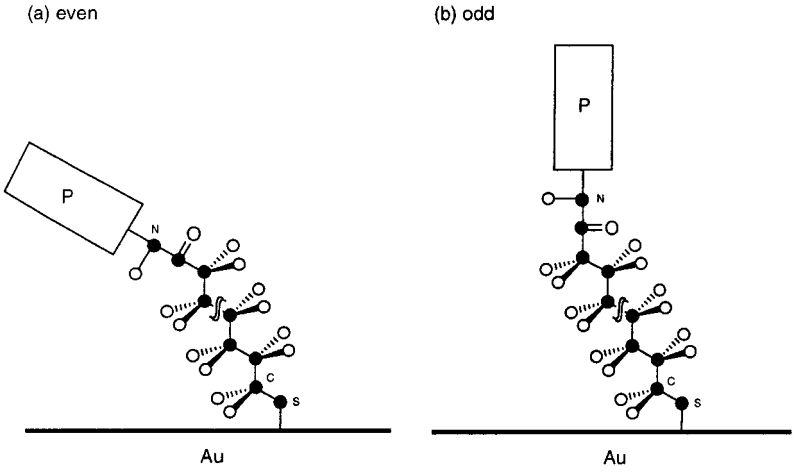

Figure 6. Proposed structures of porphyrin monolayer on Au for chains with (a) an even and (b) odd number of methylene groups.

of the porphyrin aggregation observed using the UV−visible absorption spectroscopy as well as the somewhat lower surface coverage obtained using the cyclic voltammetry, the porphyrins may be tilted from the surface normal considerably, generating the aggregation of the porphyrin for **1a**−**f**/Au/mica. Preliminary STM studies displayed small domain structures (ca. 20−40 × 20−40 Å^2) for **1a**/Au/mica. These results suggest that the structures of the monolayer are controlled by the interactions among the porphyrins as well as the length of the spacers containing the methylene chains. However, further detailed studies using AFM and STM will be necessary to elucidate the accurate structures of the porphyrin SAMs on Au(111).

There is a remarkable decrease of the fluorescence lifetimes on gold electrodes, compared with those in solutions. Bolton et al. reported fluorescence lifetime of 5-(4-carboxyphenyl)-10,-15,20-tritolylporphyrin (TTPa) in a mixed LB film with dioleoylphosphatidylcholine (DOPC) on quartz slides.[9a] At a DOPC/TTPa molar ratio of 50:1, the decay consisted primarily of one lifetime of 10.7 ns, which corresponds to monomeric TTPa in the film. The pure TTPa LB film gave three decay components (0.73 (50%), 1.3 (18%), 2.8 (32%) ns), indicating the existence of the dimer and the higher aggregates. UV−visible spectra and emission spectra of **1**/Au showed the existence of the J-aggregate like porphyrin dimer and/or the higher aggregates in the monolayers. Since the fluorescence decay on the gold surface is single component, we can conclude that the formation of the porphyrin dimer is predominant in the monolayers. However, the existence of the bulky *tert*-butyl groups on the phenyl rings at the meso positions of the porphyrin would make the interaction weaker than that of unsubstituted *meso*-tetraphenylporphyrins in LB films. Therefore, the interaction between the two porphyrins in the dimer may be weak, which is quite consistent with the relatively small red shift of the Soret band in the absorption spectra as well as the similar shape and peak position of the emission spectra on gold surface and in solutions. Synthetic porphyrin dimers in close proximity display the positive shift of the oxidation potential due to the interaction between the porphyrins.[15] However, the oxidation potentials due to the porphyrin in the monolayers are shifted more positively rather than negatively, suggesting the relatively weak interaction within the porphyrin dimer. It is known that the excited states of the dye on metal surface are strongly quenched by the metal via EN,[16] while those on glass are not quenched by the glass.[9] Based on the inconsistency of the lifetimes of the *meso*-tetraphenylporphyrins on the gold surface and glass, it is concluded that the reduction of the singlet

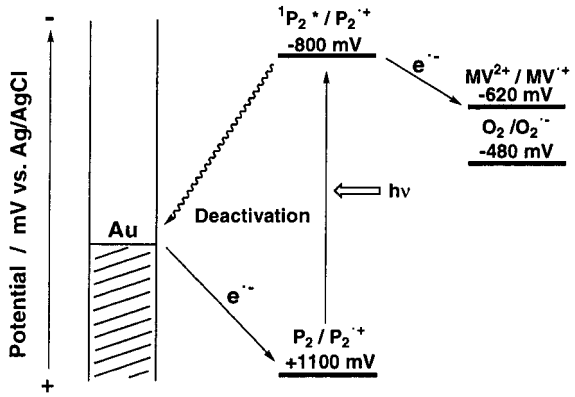

Figure 7. Photocurrent generation diagram indicating the path of electron flow.

lifetimes of the porphyrins on gold electrodes is attributed to the enhanced nonradiative decay of the excited singlet state of the dimer as well as the quenching by the gold electrodes. The weak distance dependence of the lifetimes on the gold surface seems to be the "molecular wire" behavior of the quenching through the methylene spacers between the excited singlet state of the porphyrin and the gold electrode. If the extent of the interaction in the excited singlet state of the dimer is a dominant factor for determining the lifetimes on the gold surface, the stronger interaction between the two porphyrins enhances the nonradiative decay of the excited singlet state of the dimer, thus the lifetimes on the gold surface would decrease as the number of the methylene groups increases. However, the hypothesis contradicts the experimental trend on the fluorescence lifetimes on the gold surface. Considering the weak interaction between the porphyrins, the dependence of the lifetime may be controlled by the quenching by the gold surface rather than the interaction between the porphyrins. At the present system it is quite difficult to separate the contribution of the two terms into the singlet lifetimes of the porphyrins on gold electrodes. The preliminary dilution experiment on mixed SAMs using polyalkanethiols and **1** showed still significant aggregation of the porphyrins in the monolayers, thereby making it difficult to study.

Photocurrent Generation Mechanism. Based on the above discussion, the quantum yield trend of the photocurrent generation can be explained using the following mechanism as shown in Figure 7. Assuming that the singlet and the triplet states of the porphyrin dimer in the monolayers are the same as those of the porphyrin monomer in solutions, the potentials of $^1P_2$*/$P_2^{\bullet+}$ and $^3P_2$*/$P_2^{\bullet+}$ are estimated to be −800 mV and −340 mV.

Since the redox potentials of $MV^{2+}/MV^{\bullet+}$ (−620 mV) and $O_2/O_2^{\bullet-}$ (−480 mV) are located between the two potentials, only the excited singlet state can be involved for the photoinduced ET to MV^{2+} or O_2. The reduced MV^{2+} or O_2 gives an electron to the resulting porphyrin cation radical to regenerate the ground state, or diffuses to the Pt electrode and then transfers the electron, leading to the generation of the cathodic photocurrent. However, there is a competitive deactivation pathway in the excited singlet state of the porphyrin dimer. As the number of methylenes decreases, electronic coupling between the porphyrin and the electrode increases, leading to the more efficient quenching of the excited porphyrin by the electrode via EN. In addition, the degree of the quenching may be affected by the orientation of the porphyrin planes depending on the number of the methylenes including the even-and-odd effect. Therefore, it is concluded that the zigzag progression of the quantum yield with an increase of the alkyl chain length ($n = 1-5$) is due to difference in the quenching of the excited porphyrin by the electrode depending on the spacer lengths. Creager et al. reported bridge-mediated long-range electronic coupling between ferrocene and gold in alkanethiolate-based monolayers on gold electrodes.[3c] They concluded that a donor−acceptor linked system and an electrode−donor (or acceptor) linked system are similar from the viewpoint of long-range electronic coupling in ET. Therefore, the ET rate between the porphyrin cation radical and the gold electrode becomes slower with an increase of the number of the methylene spacers. A similar distance dependence of ET rates for the aromatic and aliphatic monolayer systems has been observed experimentally.[3b,17] There would be an offset between the suppression of the quenching by the gold electrode and decrease of the ET rate between the porphyrin and the electrode with an increase of the methylene spacers. The explanation is quite consistent with the trend where the slight decrease of the quantum yield for Au/**1**/MV^{2+}/Pt cells is seen as a function of the methylene spacers ($n = 6, 7, 10, 11$). These results clearly show that optimization of each process is important to construct the highly efficient multistep ET at the organized molecular assembly mimicking photosynthetic ET.[6c]

It is interesting to compare the present system with other related systems. We have already reported the photoelectrochemical cell with the gold electrode modified with SAMs of C_{60} derivatives.[6b,c] It was shown that the vectorial anodic electron flow occurs from the electron sacrificer to the gold electrode via the excited triplet state of the C_{60}. The quantum yield (7.5−9.8%) is much higher than that in the present system. Although the separation distances between the gold electrode and the chromophores are quite similar in the C_{60} cell and Au/**1i**/MV^{2+}/Pt cell, the excited singlet state of the porphyrin is likely to be quenched much more efficiently by the gold electrode, compared to that of the C_{60}. The peculiar effect of C_{60} might be explained by the fast energy migration among the C_{60}, which is quite similar to the energy delocalization in photosynthetic antenna complexes. Aida et al. reported a series of dendrimer porphyrins bearing different numbers of five layered dendron subunits at the *meso*-positions of a porphyrin.[18] They suggested that the excitation energy migrates very efficiently over the continuous dendrimeric array of dialkoxybenzyl building units within the lifetime of the excited state. This behavior is quite similar to the energy transduction events in wheel-like arrays of chromophores in a purple photosynthetic bacterium, where the excitation energy migrates very rapidly and efficiently along the wheel, followed by transfer to the interior energy trap to initiate photoinduced charge separation events in photosynthesis.[19] Although such an energy migration seems not to be achieved in the present systems, more sophisticated design of molecular arrays on substrate using SAMs would allow us to construct light-harvesting materials.

Conclusion

The chain length effect was observed for SAMs of porphyrins using UV−visible absorption spectroscopy, cyclic voltammetry, UV−visible ellipsometry, fluorescence spectroscopy, and photoelectrochemistry. The relationship between the photoelectrochemical properties and the interfacial structure of the SAMs has been elucidated clearly for the first time. The results will provide the basic information for development of artificial photosynthetic materials as well as molecular photonics. These results are mainly based on macroscopic studies. Detailed probes of the microscopic structures using AFM and STM as well as near-edge X-ray absorption fine structure (NEXAFS) spectroscopy are in progress.

Acknowledgment. We thank Professor Tomoji Kawai and Professor Hitoshi Tabata at Osaka University for the measurements of AFM, STM, and X-ray diffraction. We are grateful to Chie Goto (TOYO Corporation) for technical assistance of the AFM measurements. This work was supported by Grants-in-Aids for COE Research and Scientific Research on Priority Areas of Electrochemistry of Ordered Interfaces (No.11118247 to H.I.) and Priority Area of Creation of Delocalized Conjugated Electronic Systems (No. 10146103 to Y.S.) from Ministry of Education, Science, Sports and Culture, Japan. Y.S. thanks the Mitsubishi Foundation for financial support.

Supporting Information Available: The synthesis and characterization of porphyrin disulfides **1**. This material is available free of charge via the Internet at http://pubs.acs.org.

References and Notes

(1) (a) Ulman, A. *An Introduction to Ultrathin Organic Films*; Academic Press: San Diego, 1991. (b) In *New Developments in Construction and Functions of Organic Thin Films*; Kajiyama, T., Aizawa, M., Eds.; Elsevier: Amsterdam, 1996. (c) In *Molecular Electronics*; Jortner, J., Ratner, M., Eds.; Blackwell: Oxford, 1997.

(2) (a) Ulman, A. *Chem. Rev.* **1996**, *96*, 1533. (b) Xia, Y.; Whitesides, G. M. *Angew. Chem., Int. Ed. Engl.* **1998**, *37*, 550.

(3) (a) Chidsey, C. E. D.; Bertozzi, C. R.; Putvinski, T. M.; Mujsce, A. M. *J. Am. Chem. Soc.* **1990**, *112*, 4301. (b) Sachs, S. B.; Dudek, S. P.; Hsung, R. P.; Sita, L. R.; Smalley, J. F.; Newton, M. D.; Feldberg, S. W.; Chidsey, C. E. D. *J. Am. Chem. Soc.* **1997**, *119*, 10563. (c) Weber, K.; Hockett, L.; Creager, S. *J. Phys. Chem. B* **1997**, *101*, 8286.

(4) (a) Caldwell, W. B.; Campbell, D. J.; Chen, K.; Herr, B. R.; Mirkin, C. A.; Malik, A.; Durbin, M. K.; Dutta, P.; Huang, K. G. *J. Am. Chem. Soc.* **1995**, *117*, 6071. (b) Campbell, D. J.; Herr, B. R.; Hulteen, J. C.; Van Duyne, R. P.; Mirkin, C. A. *J. Am. Chem. Soc.* **1996**, *118*, 10211. (c) Ye, Q.; Fang, J.; Sun, L. *J. Phys. Chem. B* **1997**, *101*, 8221.

(5) (a) Zak, J.; Yuan, H.; Ho, M.; Woo, L. K.; Porter, M. D. *Langmuir* **1993**, *9*, 2772. (b) Uosaki, K.; Kondo, T.; Zhang, X.-Q.; Yanagida, M. *J. Am. Chem. Soc.* **1997**, *119*, 8367. (c) Imahori, H.; Norieda, H.; Ozawa, S.; Ushida, K.; Yamada, H.; Azuma, T.; Tamaki, K.; Sakata, Y. *Langmuir* **1998**, *14*, 5335.

(6) (a) Mirkin, C. A.; Caldwell, W. B. *Tetrahedron* **1996**, *52*, 5113. (b) Imahori, H.; Azuma, T.; Ajavakom, A.; Norieda, H.; Yamada, H.; Sakata, Y. *J. Phys. Chem. B* **1999**, *103*, 7233. (c) Imahori, H.; Sakata, Y. *Eur. J. Org. Chem.* **1999**, 2445.

(7) (a) Finklea, H. O.; Hanshew, D. D. *J. Am. Chem. Soc.* **1992**, *114*, 3173. (b) Doron, A.; Portnoy, M.; Lion-Dagan, M.; Katz, E.; Willner, I. *J. Am. Chem. Soc.* **1996**, *118*, 8937. (c) Fox, M. A. *Acc. Chem. Res.* **1999**, *32*, 201.

(8) Yamazaki, I.; Tamai, N.; Kume, H.; Tsuchiya, H.; Oba, K. *Rev. Sci. Instrum.* **1985**, *56*, 1187.

(9) (a) Dick, H. A.; Bolton, J. R.; Picard, G.; Munger, G.; Leblanc, R. M. *Langmuir* **1988**, *4*, 133. (b) Gust, D.; Moore, T. A.; Moore, A. L.; Luttrull, D. K.; DeGraziano, J. M.; Boldt, N. J.; Van der Auweraer, M.; De Schryver, F. C. *Langmuir* **1991**, *7*, 1483. (c) Choudhury, B.; Weedon, A. C.; Bolton, J. R. *Langmuir* **1998**, *14*, 6192.

(10) (a) Akins, D. L.; Özçelik, S.; Zhu, H.-R.; Guo, C. *J. Phys. Chem.* **1996**, *100*, 14390. (b) Maiti, N. C.; Mazumdar, S.; Periasamy, N. *J. Phys. Chem. B* **1998**, *102*, 1528. (c) Khairutdinov, R. F.; Serpone, N. *J. Phys. Chem. B* **1999**, *103*, 761.

(11) Osuka, A.; Maruyama, K. *J. Am. Chem. Soc.* **1988**, *110*, 4454.

(12) It is known that densely packed monolayer films exhibit inhibited ion transport and reduced electrochemical accessibility.[4b] Thus, coverage (Γ) is a low limit estimate and occupied area is an upper limit estimate. Considering that the porphyrins are planar large molecules with bulky substituents at the meso positions, even in the densely packed monolayer films the electrochemical accessibility may be similar to that in the ideal system where surface-confined redox-active molecules are completely electrochemically accessible in the film.

(13) (a) Walczak, M. M.; Chung, C.; Stole, S. M.; Widrig, C. A.; Porter, M. D. *J. Am. Chem. Soc.* **1991**, *113*, 2370. (b) Bryant, M. A.; Pemberton, J. E. *J. Am. Chem. Soc.* **1991**, *113*, 8284.

(14) Sugiura, K.-i.; Iwasaki, K.; Umishita, K.; Hino, S.; Ogata, H.; Miyajima, S.; Sakata, Y. *Chem. Lett.* **1999**, 841.

(15) Osuka, A.; Nakajima, S.; Maruyama, K. *J. Org. Chem.* **1992**, *57*, 7355.

(16) (a) Chance, R. R.; Prock, A.; Silbey, R. *Adv. Chem. Phys.* **1978**, *37*, 1. (b) Waldeck, D. H.; Alivisatos, A. P.; Harris, C. B. *Surf. Sci.* **1985**, *158*, 103. (c) Zhou, X.-L.; Zhu, X.-Y.; White, J. M. *Acc. Chem. Res.* **1990**, *23*, 327. (d) Cnossen, G.; Drabe, K. E.; Wiersma, D. A. *J. Chem. Phys.* **1993**, *98*, 5276.

(17) Finklea, H. O. In *Electroanalytical Chemistry*; Bard, A. J., Rubinstein, I., Eds.; Marcel Dekker: New York, 1996; Vol. 19, p 109−335.

(18) Jiang, D.-L.; Aida, T. *J. Am. Chem. Soc.* **1998**, *120*, 10895.

(19) (a) Mcdermontt, G.; Prince, S. M.; Freer, A. A.; Hawthornthwaite-Lawless, A. M.; Rapiz, M. Z.; Cogdell, R. J.; Isaacs, N. W. *Nature* **1995**, *374*, 517. (b) Kuhlbrandt, W. *Nature* **1995**, *374*, 497.